CDF note 11083

A Measurement of the Ratio $\frac{\sigma(B_c^+)*BR(B_c^+\to J/\psi\mu^+\nu)}{\sigma(B^+)*BR(B^+\to J/\psi K^+)}$ Using the Complete CDF Dataset

The CDF Collaboration
URL http://www-cdf.fnal.gov
(Dated: March 10, 2014)

This note describes the B_c^+ production cross section times branching ratio measurement of the decay mode $B_c^+ \to J/\psi\mu^+\nu$ relative to the $B^+ \to J/\psi K^+$ decay. Measurements are based on the complete CDF run II data set that for this measurement consists of an integrated luminosity of 8.7 fb^{-1}. We select a sample of 1370 events in which a J/ψ candidate is matched with a high quality third muon and the J/ψ decays to two muons for $p_T(B_c^+) > 6$ GeV/c. The background contributions from misidentified J/ψ, misidentified muons, and from the different b-hadrons are estimated using data and PYTHIA samples. The total background consists of 630.5±14.2 events. We estimate the ratio of the production cross section times branching ratio of $B_c^+ \to J/\psi\mu^+\nu$ relative to $B^+ \to J/\psi K^+$ for $p_T(B_c^+) > 6$ GeV/c and $|y| < 0.6$ as 0.211 ± 0.012 (stat.)$^{+0.021}_{-0.020}$ (syst.).

Preliminary Results for Spring 2014 Conferences

I. INTRODUCTION

The B_c^+ meson is the most massive of the bottom-flavored mesons, apart from the $b\bar{b}$ charmonia, with a ground state that consists of a $\bar{b}$ and a c quark [1]. The B_c^+ meson was discovered by CDF in Run I using the $B_c^+ \to J/\psi \ell^+ X$ decay modes [2]. The ratio of the B_c^+ production cross section times semileptonic branching ratio in the single muon and electron channels to the production cross section times branching ratio for $B^+ \to J/\psi K^+$ using an integrated luminosity of 360 pb^{-1} of Run II data was presented in Refs. [3] and [4], respectively. A similar measurement in the muon channel using an integrated luminosity of 1 fb^{-1} of Run II data was presented in [5]. Measurements of the B_c^+ lifetime in the $B_c^+ \to J/\psi \mu^+ X$ and $B_c^+ \to J/\psi e^+ X$ decay channels using an integrated luminosity of 1 fb^{-1} of Run II data was presented in [6]. In this note we update the $\frac{\sigma(B_c^+) * BR(B_c^+ \to J/\psi \mu^+ \nu)}{\sigma(B^+) * BR(B^+ \to J/\psi K^+)}$ ratio to include the full CDF run II dataset, which for this measurement has an integrated luminosity of (8.7 ± 0.5) fb^{-1}.

II. EVENT SELECTION

The datasets used in this analysis are collected with the J/ψ di-muon trigger and consist of an integrated luminosity of 8.7 fb^{-1}. Our selection requirements closely follow those of the earlier B_c^+ semileptonic cross-section [5] and lifetime measurements [6], in which we search for J/ψ particles reconstructed through the $\mu^+\mu^-$ decay channel that are matched with a third track associated with the J/ψ vertex. The third track might be:

- the muon in the $B_c^+ \to J/\psi \mu^+ X$ decays, or
- the kaon in the $B^+ \to J/\psi K^+$ sample, or
- a π^+, K^+ or p for the misidentified muon background calculation

Since the luminosity increases over the time of taking data, we expect that our B_c^+ and B^+ yields will vary versus the calendar time due to the J/ψ dimuon trigger prescale modification. The question arises as to how stable the ratio of the B_c^+ to B^+ yields are as a function of time. Figure 1 shows the ratio of B_c^+ to B^+ yields versus the dataset section number. A fit to the ratio $N(B_c^+)/N(B^+)$

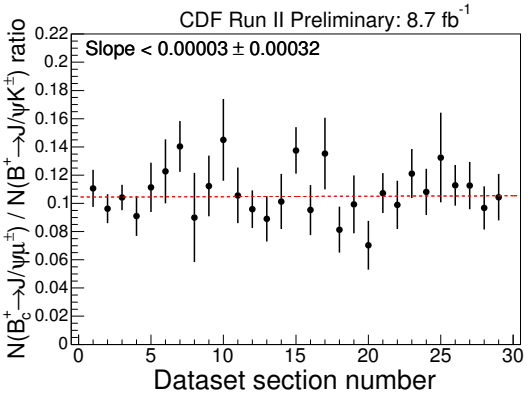

FIG. 1: The ratio of B_c^+ to B^+ yields versus the dataset section number.

shown in Fig. 1 yields the slope value 0.00003±0.00032 consistent with zero.

The invariant mass distributions of the $J/\psi\mu^+$ and $J/\psi K^+$ event candidates are shown in Fig. 2. There are 1,370 $B_c^+ \to J/\psi \mu^+ \nu$ event candidates within a $4-6$ GeV/c^2 signal mass window and 14,338 ± 125 events from $B^+ \to J/\psi K^+$ decays. The fit function for the $J/\psi K^+$ invariant mass

distribution consist of: a double Gaussian for $B^+ \to J/\psi K^+$ decays, a mass template for the Cabibbo suppressed $B^+ \to J/\psi\pi^+$ contribution within the mass range 5.28-5.4 GeV/c^2 based on Monte Carlo simulation, and a second order polynomial for the continuum background. The Cabibbo suppressed $B^+ \to J/\psi\pi^+$ contribution is fixed to 3.83% of N($B^+ \to J/\psi K^+$) following Ref. [7]. In order to

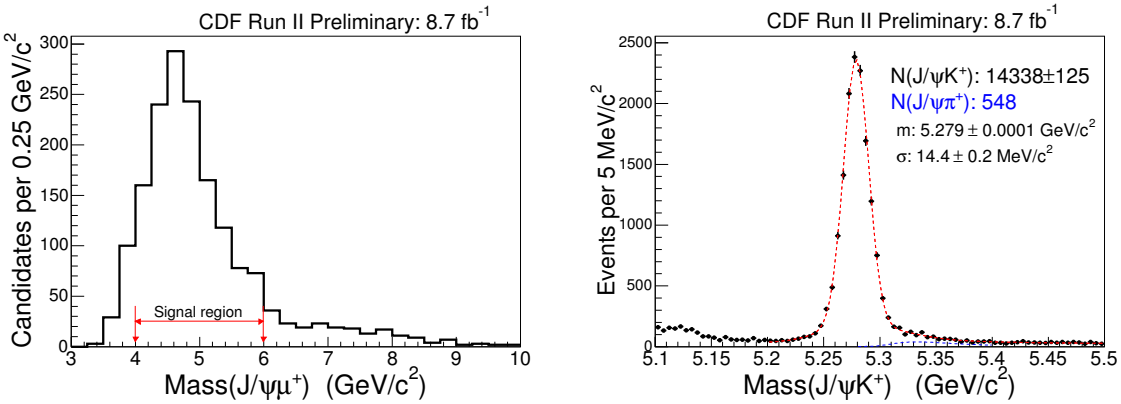

FIG. 2: The invariant mass distributions of the $J/\psi\mu^+$ (left) and $J/\psi K^+$ (right). The B_c^+ signal region lies between 4 and 6 GeV/c^2 (left). The Cabibbo suppressed $B^+ \to J/\psi\pi^+$ contribution is shown as a dashed blue curve (right). N($B^+ \to J/\psi\pi^+$) is fixed to 3.83% of N($B^+ \to J/\psi K^+$) following Ref. [7].

determine the number of B_c^+ signal events, we must calculate the background contributions to the sample and subtract them from the number of candidates.

III. B_C^+ BACKGROUND

We consider the following background sources to the semileptonic B_c^+ decays:

- Misidentified J/ψ
- Misidentified third muon
- $b\bar{b}$ background
- Contributions from other decay modes

A. Misidentified J/ψ background

The number of misidentified J/ψ plus a third muon is estimated using the di-muons from the sidebands of the J/ψ invariant mass distribution. Our signal di-muon mass region is within ± 0.05 GeV/c^2 around the PDG mean value of the J/ψ mass, $m_{J/\psi}$. The selected sideband regions are: $|m_{J/\psi} - 0.150$ GeV/$c^2| < 0.05$ GeV/c^2 and $|m_{J/\psi} + 0.150$ GeV/$c^2| < 0.05$ GeV/c^2. The resulting invariant mass distributions of the $J/\psi_{side}\mu^+$ system can be seen in Fig. 3. We find 11.5±2.4 events below 4 GeV/c^2, 96.5±6.9 events within the $4-6$ GeV/c^2 signal mass window and 25±3.5 events > 6 GeV/c^2.

B. Misidentified muon background

The misidentified muon contribution to the B_c^+ background is calculated using the following steps:

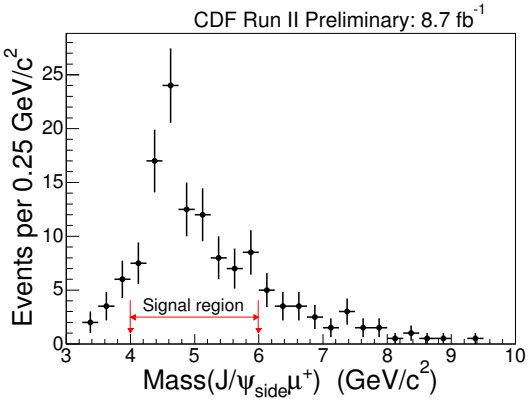

FIG. 3: The invariant mass distributions of the $J/\psi_{side}\mu^+$ system.

- Reconstruct the $J/\psi track$ system to use as an input sample for the misidentified muon calculation.
- Determine the kaon and pion decay-in-flight and punch-through probabilities from a D^* sample having the decay chain $D^* \to D^0\pi^+$, $D^0 \to K^-\pi^+$ using the two track trigger datasets.
- Determine the fraction of the events outside of the D^0 mass peak using Monte Carlo simulation.
- Determine the pion, kaon, and proton fractions in the $J/\psi track$ data using dE/dx and time-of-flight tools.

The invariant mass distribution of the $J/\psi track$ system is shown in Fig. 4. In the fit procedure the muon mass was assigned to the third track. For each third track in this sample we assign a weight W to calculate the misidentified muon background:

$$W = \epsilon_\pi \cdot (1 + F_\pi^{out}) \cdot F_\pi + \epsilon_K \cdot (1 + \alpha F_K^{out}) \cdot F_K + \epsilon_p \cdot F_p, \quad (1)$$

where $\epsilon_{(\pi,K,p)}$ is the probability for a given particle type to be misidentified as a muon, $F_{\pi,K}^{out}$ is the fraction of misidentified events outside of the D^0 mass peak for a given particle type, α=1 for K^-, $\alpha = \epsilon_{K^-}/\epsilon_{K^+}$ for K^+, and F(π, K, p) is the fraction of a given particle type within the $J/\psi track$ sample. The weight W is applied on a track-by-track basis to calculate the weighted $J/\psi track$ mass distribution.

The misidentification probabilities derived from data assume that the π/K track, even after a possible kink in the $\pi(K) \to \mu + X$ decay-in-flight, will allow the reconstructed D^0 mass value to remain under the peak. The fraction of the events outside of the D^0 mass peak are accounted for with a special simulation study.

The proton probability to make a misidentified muon via the punch-through process is estimated using the proton tracks in $\Lambda \to p\pi$ decays. We are able to establish only an upper limit for this process since it is so rare.

The muon misidentification probabilities and the fraction of the muon associated events outside of the D^0 mass peak as a function of hadron p_T are shown in Fig. 5.

The π fraction F_π in the $J/\psi track$ sample is determined using a dE/dx method. The K and p energy losses in the COT for our $p_T > 3$ GeV/c range are insufficient to separate them in the dE/dx distribution. Consequently, the K and p fractions F_{K+p} are combined. The proton fraction F_p is estimated only within the $2 - 3$ GeV/c momentum region using a simultaneous fit of the dE/dx and time-of-flight data. For higher momenta ($p > 3$ GeV/c) we follow the predictions for F_p from PYTHIA.

In order to estimate the π and $K + p$ fractions, we initially intended to fit the dE/dx distribution with two Gaussians, where the mean for the pion's is zero and the mean for $K + p$ is about -1.5.

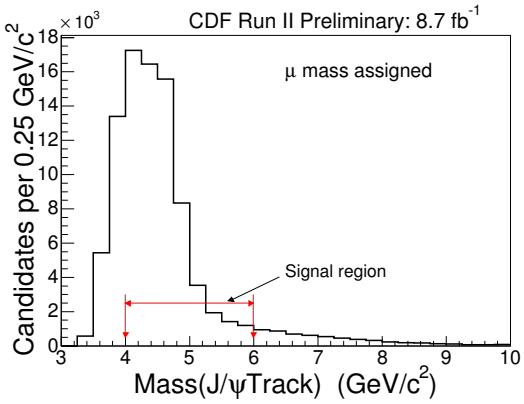

FIG. 4: The invariant mass distribution of the $J/\psi track$ system. This sample is an input to the misidentified muon calculation.

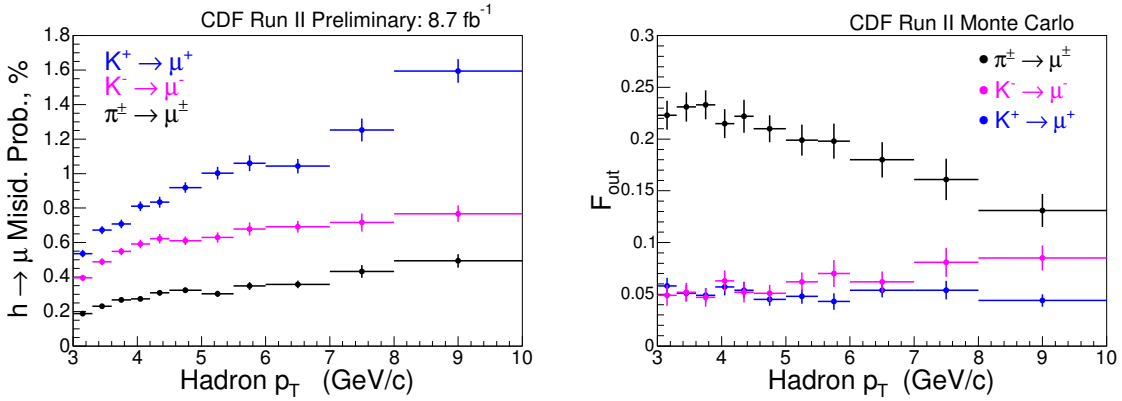

FIG. 5: The $\pi^{\pm}$ and $K^{\pm}$ muon misidentification probabilities (left) and the fraction of the muon associated events outside of the D^0 mass peak (right) as a function of hadron p_T.

However, we are faced with the challenge that the sum of two single Gaussians does not well describe the pion's positive tail, or the kaon's either. As another option we considered the use of a Gamma distribution. Finally, the the dE/dx data were fitted with following formula:

$$N_{ev} = N_{fit} * [F_\pi \times \mathrm{GPDF}(\gamma_\pi, \mu_\pi, \beta_\pi) + (1 - F_\pi) \times \mathrm{GPDF}(\gamma_{K+p}, \mu_{K+p}, \beta_{K+p})], \quad (2)$$

where N_{fit} is the number of events, F_π is the pion fraction, $F_{K+p} = 1 - F_\pi$, and GPDF is the probability density function of the Gamma distribution. There are only two free parameters in the fit: N_{fit} and F_π. The rest of the quantities are fixed: $\gamma_\pi = 6.8$, $\beta_\pi = \frac{1.11}{\sqrt{\gamma_\pi}}$, and $\mu_\pi = -\gamma_\pi\beta_\pi$ for pions; $\gamma_{K+p} = 23$, $\beta_{K+p} = \frac{1.15}{\sqrt{\gamma_{K+p}}}$, and $\mu_{K+p} = kpMean - \gamma_{K+p}\beta_{K+p}$ for $K + p$, where $kpMean$ is the $K + p$ momentum dependent position with respect to the pion and changes slowly for each specific momentum bin. These settings will lead to the mean for the pion to be zero, the mean for the $K + p$ to be $kpMean$, and widths of 1.11 and 1.15 for pions and $K + p$, respectively. Figure 6 shows the distributions of the dE/dx data for the positively charged tracks in various momentum ranges. The Gamma distribution for kaon's alone is well calibrated by using dE/dx data from an independent sample of $B^+ \to J/\psi K^+$ events.

Figure 7 shows the F_π, F_K, and F_p fractions for the positively (left) and negatively (right) charged third tracks for the $J/\psi track$ system for track momenta > 3 GeV/c.

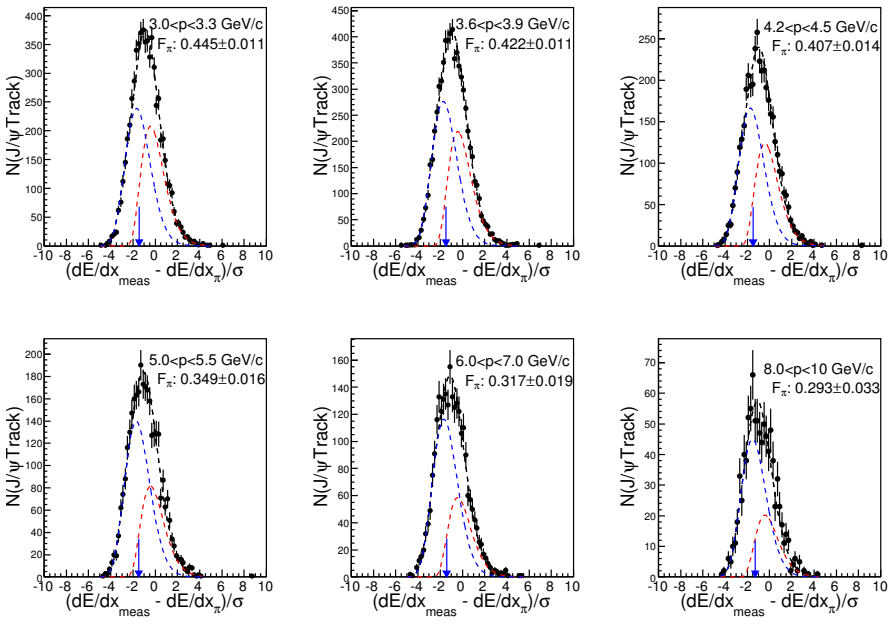

FIG. 6: The distributions of the dE/dx data for the positively charged tracks in various momentum ranges. The fitted function consists of two Gamma distributions, one for pions and a second one for the combined $K+p$. The parameters are: $\gamma_\pi = 6.8$, $\beta_\pi = \frac{1.11}{\sqrt{\gamma_\pi}}$, and $\mu_\pi = -\gamma_\pi\beta_\pi$ for pions; $\gamma_{K+p} = 23$, $\beta_{K+p} = \frac{1.15}{\sqrt{\gamma_{K+p}}}$, and $\mu_{K+p} = kpMean - \gamma_{K+p}\beta_{K+p}$ for $K+p$, where $kpMean$ is the $K+p$ momentum dependent position with respect to the pion and changes slowly for each specific momentum bin. The fit returns the F_π for pions, where the fraction F_{K+p} is defined as 1 - F_π.

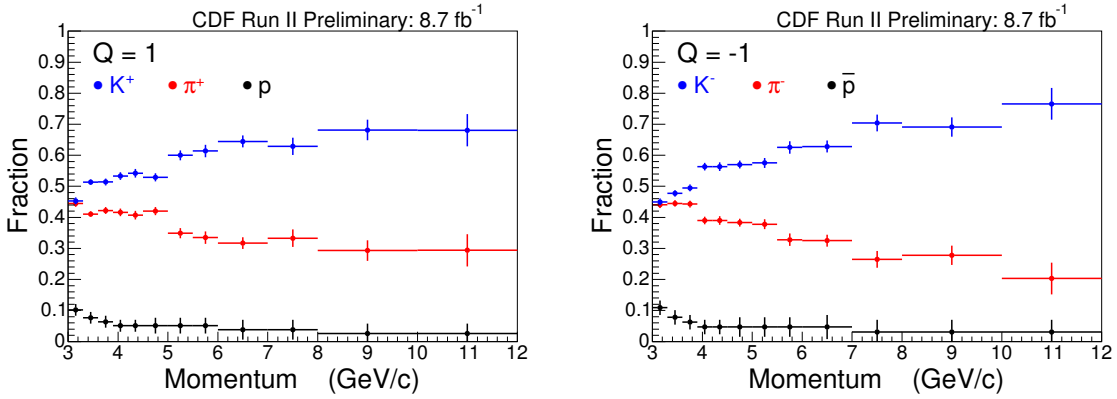

FIG. 7: The fractions F_π, F_K, and F_p for the positively (left) and negatively (right) charged third tracks for the $J/\psi track$ system for track momenta >3 GeV/c.

For the misidentified muon uncertainties the following options were considered to estimate the various components of the systematic uncertainty:

- For the π/K muon misidentification probabilities, the daughter distributions associated with a high quality muon are fitted with the double Gaussian templates derived from the non-muon sample and compared with the results from the single Gaussian fits.

- For the fraction of the muon associated events outside of the D^0 mass peak, the Monte Carlo mass distributions fitted with single Gaussians forced to have the same widths as the experimental data and were compared with single Guassian fits where the Monte Carlo simulation was allowed to set the widths of the fits. The resulting differences are used to estimate the systematic uncertainty for this part of the mididentified muon calculation.

- For the particle fractions (π and $K+p$) in the $J/\psi track$ system, fits of the dE/dx data with a single Gaussian function are compared to the fits with Gamma distributions to determine the systematic uncertainty.

- For the proton fractions, the data normalized PYTHIA simulation is bounded conservatively from above and below to determine the systematic uncertainty. From below we follow the slope of the Pythia smulation in the region 3-4.2 GeV/c assuming that $F_p = 0$ beyond 5.5 GeV/c. From above we assume a straight line connecting the lowest and highest momentum points in the Pythia simulation (see the dashed lines in Fig. 8).

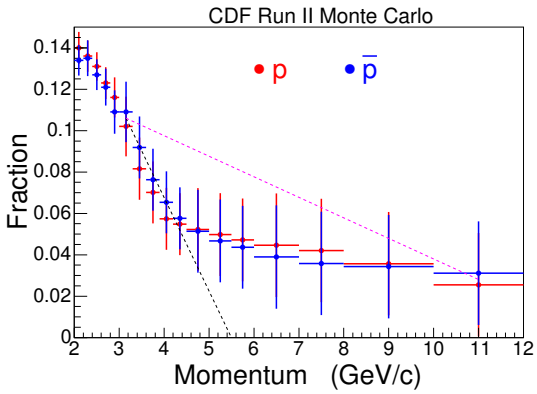

FIG. 8: The F_p fractions for the charged third tracks of the $J/\psi track$ system. The dashed lines are used for the systematic uncertainty studies.

Both the misidentified J/ψ and misidentified muon backgrounds have one common subsample: misidentified J/ψ with a misidentified third μ. To avoid double counting, it is necessary to subtract it only once. To calculate the doubly fake background, we apply the same weighting procedure to the sideband J/ψ plus track sample using the misidentification probabilities and the π, K, and p fractions.

The misidentified muon and "double fake" backgrounds versus the invariant mass value of the $J/\psi track$ system and the associated systematic uncertainties are shown in Fig. 9. The numerical results are given in Table I.

"Misidentified" backgrounds	$M < 4$ GeV/c^2	$4 < M < 6$ GeV/c^2	$M > 6$ GeV/c^2
Misidentified muon	$86.7^{+2.4}_{-4.2}$	$344.4^{+9.6}_{-16.5}$	$32.1^{+0.9}_{-1.5}$
Double fake	$5.1^{+0.1}_{-0.2}$	$19.0^{+0.5}_{-0.9}$	$5.2^{+0.1}_{-0.3}$

TABLE I: The misidentified muon and "double fake" backgrounds within the signal and sideband mass regions and the associated systematic uncertainties.

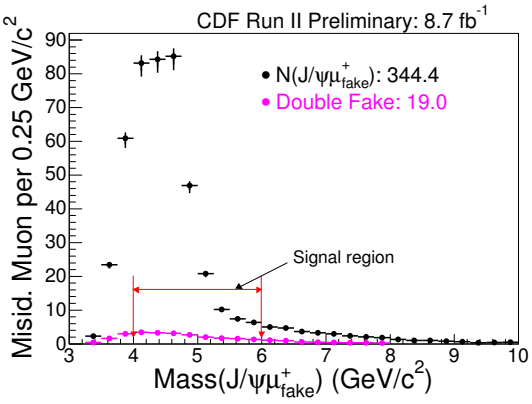

FIG. 9: The weighted invariant mass distribution of the $J/\psi track$ system showing the misidentified muon (black) and the "double fake" (pink) backgrounds to the $B_c^+ \to J/\psi\mu^+$ decays. The error bars represents the estimated systematic uncertainties. Because of the large size of the $J/\psi track$ sample, the statistical errors in the misidentified muon calculation are negligible.

C. The $b\bar{b}$ background

We must also account for cases when the J/ψ is produced by a b hadron and the third muon is produced by a $\bar{b}$ hadron (or vice versa) in the same event. The basic procedure for the calculation is described in the semileptonic B_c^+ lifetime measurement [6]. However, we updated many steps of this calculation. Therefore, we describe the full procedure here. The $b\bar{b}$ background calculation is based on a PYTHIA Monte Carlo simulation. The question is what fractions of QCD production processes "flavor creation" (FC), "flavor excitation" (FE), and "gluon splitting" (GS) should be used in determining the $b\bar{b}$ backgound for $B_c^+ \to J/\psi\mu^+\nu$ decays. A lengthy study led to the conclusion that a more expermimentally driven choice is to constrain the QCD fractions by requiring them to give a good description of the $\Delta\phi$ distributions for the unvertexed $J/\psi\mu^+$ pairs in the experimental data. Fig. 10 shows the $\Delta\phi$ distributions of all unvertexed $J/\psi\mu^+$ pairs from data (left), the three non-$b\bar{b}$ contributions to the left plot superimposed (middle,) and the left plot with the non-$b\bar{b}$ contributions and all events which pass the vertex probability requirement subtracted (right).

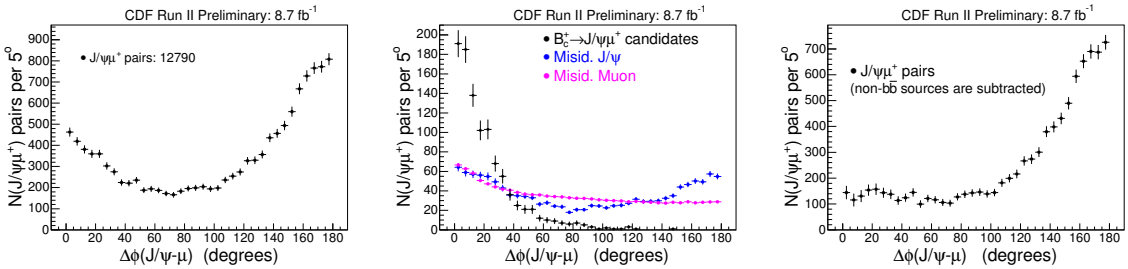

FIG. 10: The $\Delta\phi$ distributions of all unvertexed $J/\psi\mu^+$ pairs from data (left), the three non-$b\bar{b}$ contributions to the left plot superimposed (middle), and the left plot with the non-$b\bar{b}$ contributions and all events which pass the vertex probability requirement subtracted (right). The plots represent the complete CDF dataset.

Using the PYTHIA generator, we simulate the J/ψ production from one b hadron and force the other $\bar{b}$ hadron in the same event to decay semileptonically via a muon. The b hadron decaying to the J/ψ includes the $J/\psi K^+$ decay chain.

The fit of the $\Delta\phi$ distributions shown in the Fig. 10 (right) with all three QCD production mechanisms lead to the result where the experimental data rejected the "flavor excitation" contribution.

The fit returned for the associated FE scale factor the value S_{FE} = -0.11±0.10. Therefore, we fit the $\Delta\phi$ distribution determined from data using only the FC and GS contributions. The predicted number of $b\bar{b}$ events, $N_{b\bar{b}}^{pred}$ for a given $\Delta\phi$ bin is given by the formula:

$$N_{b\bar{b}}^{pred} = C_{norm}(S_{FC}N_{b\bar{b}}^{FC} + S_{GS}N_{b\bar{b}}^{GS}) \times \frac{N_{B^+}^{data}}{S_{FC}N_{B^+}^{FC} + S_{GS}N_{B^+}^{GS}}, \quad (3)$$

Here, C_{norm} = 0.76±0.07 is a parameter that accounts for the uncertainties in the simulation of J/ψ production in B decays relative to the $B^+ \to J/\psi K^+$ branching fraction. In the fit the value of C_{norm} is constrained by it's uncertainty. The parameters S_{FC} and S_{GS} are the scale factors for the FC and GS QCD processes in PYTHIA. The fit procedure allows the scale factors to float. $N_{b\bar{b}}^{FC}$ and $N_{b\bar{b}}^{GS}$ are the number of PYTHIA events in a given $\Delta\phi$ bin from FC and GS, respectively. $N_{B^+}^{data}$ is the total number of $B^+ \to J/\psi K^+$ decays in the data shown in Fig. 2 (right). $N_{B^+}^{FC}$ and $N_{B^+}^{GS}$ are the numbers of $B^+ \to J/\psi K^+$ decays produced by the two QCD processes in PYTHIA. This last term provides for the normalization of the PYTHIA sample to data.

Figure 11 shows the result of the fit to the $\Delta\phi$ distribution presented in Fig. 10 (right) with the two QCD production mechanisms FC and GS. The results of the fits are shown in Table II.

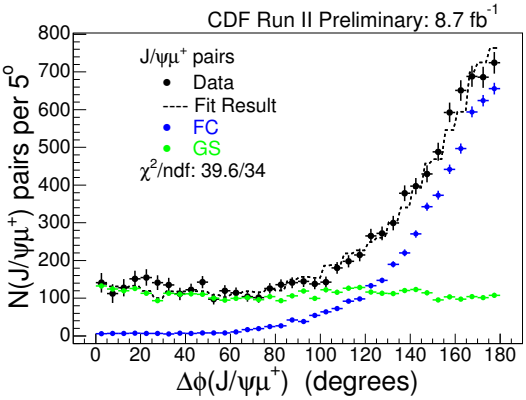

FIG. 11: The fit of the $b\bar{b}$ distribution from unvertexed $J/\psi\mu^+$ data using FC (blue) and GS (green) QCD predictions.

C_{norm}	0.73±0.01
S_{FC}	2-S_{GS}
S_{GS}	1.02±0.03
χ^2/ndf	39.6/34

TABLE II: The fit results for the data shown in Fig. 11. The expected value for C_{norm} is 0.76±0.07. The fit parameters are used to calculate the central value of the $b\bar{b}$ background.

The final results for the $b\bar{b}$ background in the signal region are summarized in Table III. The uncertainty in the $b\bar{b}$ background is due to several sources. There are statistical uncertainties in the four PYTHIA simulated samples: $N_{b\bar{b}}^{FC}$, $N_{b\bar{b}}^{GS}$, $N_{B^+}^{FC}$, and $N_{B^+}^{GS}$. There is the statistical uncertainty in the determination of the $B^+ \to J/\psi K^+$ sample in the experimental data. Finally there are uncertainties in the parameters C_{norm}, S_{FC} and S_{GS} that are determined by the fit to the $\Delta\phi$ distribution in the unvertexed $J/\psi\mu^+$ sample plus additional correlations between all these quantities that are introduced by the fitting procedure. The resulting invariant mass distribution of the $b\bar{b}$ background is shown in Fig. 12.

Flavor creation (FC)	12.9 ± 4.1
Flavor excitation (FE)	0
Gluon splitting (GS)	165.7 ± 11.7
Total	178.6 ± 12.4

TABLE III: The expected number of $b\bar{b}$ background events in the signal region. Uncertainties are statistical due to the sizes of the three muon systems, the number of B^+, and the statistical uncertainty of the scale factors.

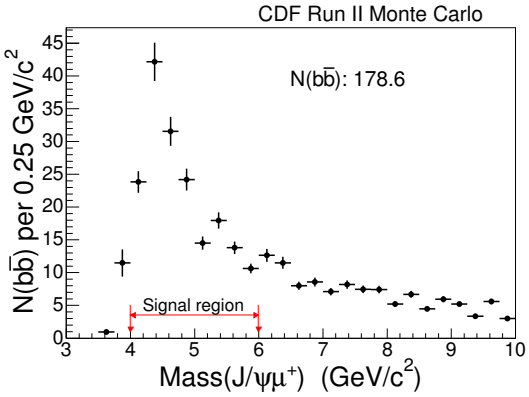

FIG. 12: The invariant mass distribution of the $b\bar{b}$ background. The error bars represent the statistical uncertainties.

As an estimate of the systematic uncertainty, we use the differences between the two values for S_{FE}: 0 and 0.1. As another source of systematic uncertainty we vary the systematic uncertainty of the unvertexed misidentified muon within $\pm 1\sigma$ of it's value in each $\Delta\phi$ bin. These variation lead to the rising and lowering of the unvertexed $\Delta\phi(J/\psi\mu^+)$ distribution shown in Fig. 10 (right).

Finally, the $b\bar{b}$ background in the high and low mass regions outside of the signal region is 12.4 ± 2.4 within the $3-4$ GeV/c^2 and 110.4 ± 10.7 within the $>$ 6GeV/c^2 mass region. The final $b\bar{b}$ background in the signal mass region and it's statistical and systematic uncertainty is 178.6 ± 12.4(stat) ± 5.8(sys).

D. Summary of the backgrounds

The summary of the backgrounds described above along with the statistical uncertainties are shown in Table IV. It includes the misidentified J/ψ, misidentified muon, and $b\bar{b}$ backgrounds. The doubly misidentified contribution is subtracted to avoid double counting.

Backgrounds	$M < 4$ GeV/c^2	$4 < M < 6$ GeV/c^2	$M > 6$ GeV/c^2
Misidentified J/ψ	11.5 ± 2.4	96.5 ± 6.9	25 ± 3.5
Misidentified muon	86.7	344.4	32.1
Double fake	-5.1	-19.0	-5.2
$b\bar{b}$ background	12.4 ± 2.4	178.6 ± 12.4	110.4 ± 10.7
Sum of Misid.+bb	105.5 ± 3.4	600.5 ± 14.2	162.3 ± 11.3

TABLE IV: Summary of the misidentified J/ψ, misidentified muon, double fake, and $b\bar{b}$ backgrounds. The doubly misidentified contribution is subtracted to avoid double counting. All uncertainties are statistical.

The excess of the $B_c^+ \to J/\psi\mu^+X$ candidates over the backgrounds described above, N_{obs}, is presented in Table V. The top line in Table V represents the reconstructed number of $B_c^+ \to J/\psi\mu^+X$ candidates shown in Fig. 2 (left). The quantity N_{obs} is used to calculate the final $B_c^+ \to J/\psi\mu^+\nu$ yield.

	$3-4$ GeV/c^2	$4-6$ GeV/c^2	$>$ 6GeV/c^2
$N(B_c^+ \to J/\psi\mu^+X)$, reconstr.	132 ± 11.5	1370 ± 37.0	208 ± 14.4
Sum of Misid.+$b\bar{b}$ backgr.	105.5 ± 3.4	600.5 ± 14.2	162.3 ± 11.3
N_{obs}	26.5 ± 12.0	769.5 ± 39.6	45.7 ± 18.3

TABLE V: The excess of the $B_c^+ \to J/\psi\mu^+X$ candidates over the backgrounds described above.

IV. CONTRIBUTIONS FROM OTHER DECAY MODES

After subtracting the backgrounds, the basic tri-muon sample that is reconstructed from data may still have contributions from other B_c^+ decay modes. For example, a B_c^+ might decay into $\psi(2S) + \mu^+ + \nu$ followed by $\psi(2S)$ decay into $J/\psi + ...$ Another example is a B_c^+ decay into $J/\psi + \tau^+ + \nu$ followed by the τ decay into a muon. The probability of events from these decays to survive our selection requirements is small, but non-zero.

In order to determine contributions from other decay modes, we generate 2.2×10^7 $B_c^+ \to J/\psi\mu^+X$ decays associated with 11 other decay modes that may end-up in the tri-muon system. The branching fractions of these decay modes are taken from theoretical predictions [8].

Our method uses the number of observed B_c^+ candidates, N_{obs}, in the data after all the other backgrounds have been subtracted except for the other decay modes as shown in Table V. The number of $B_c^+ \to J/\psi\mu^+\nu$ events in the data is given by $N_{B_c^+} = N_{obs} - N_{other}$ where N_{other} is the number due to other decay modes. Study shows that the surviving fractions of the other decay modes combined with respect to the $B_c^+ \to J/\psi\mu^+\nu$ channel are: 9.9% in the $3-4$ GeV/c^2 mass range, 3.9% in the signal mass range, and no contribution in the $>$ 6GeV/c^2 mass range. Finally, the other decays are: 769.5×(1-0.961) = 30.0 in the signal mass range and 26.5×(1-0.901) = 2.6 events in the $3-4$ GeV/c^2 mass range.

Note that the the surviving fractions of the other decay modes based on the prediction [9] are: 7.5% in the $3-4$ GeV/c^2 mass range, 2.6% in the signal mass range, and no contribution in the $>$ 6GeV/c^2 mass range. Then, the Ivanov prediction for other decay modes is 769.5×(1-0.974) = 20.0 events.

V. THE B_C^+ EXCESS

The N_{obs} from Table V is used as an input to calculate the other decay modes contribution. The other decay modes and the B_c^+ excess, $N_{B_c^+}$, is shown in Table VI.

The invariant mass distribution of the $J/\psi\mu^+$ candidate events is shown in Fig. 13 with Monte Carlo simulated signal and the backgrounds superimposed. "Misid. Muon" stands for the misidentified muon background with the doubly misidentified background subtracted, while "Other modes" indicates the contribution from the the other decay modes. "B_c Monte Carlo" stands for the simulated $B_c^+ \to J/\psi\mu^+\nu$ decays. The simulated sample size is set to the number of signal events in the data after background subtraction.

	$3-4$ GeV/c^2	$4-6$ GeV/c^2	$>$ 6GeV/c^2
N_{obs}	26.5 ± 12.0	769.5 ± 39.6	45.7 ± 18.3
Other decay modes	2.6 ± 0.1	30.0 ± 0.2	0
$N_{B_c^+}$	23.9 ± 12.0	739.5 ± 39.6	45.7 ± 18.3
$N(B_c^+ \to J/\psi\mu^+\nu)$, Monte Carlo	22.8 ± 0.6	739.5 ± 3.7	27.6 ± 0.06

TABLE VI: B_c^+ excess from the $B_c^+ \to J/\psi\mu^+\nu$ decay, $N_{B_c^+}$. All uncertainties are statistical. The last line presents the Monte Carlo simulated events in the different mass regions, they are scaled down so that the number in the signal region is consistent with the experimental data.

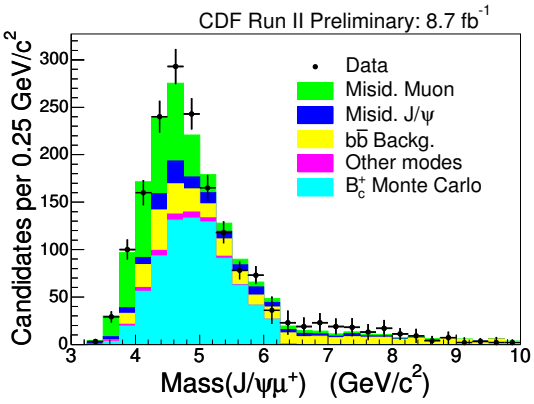

FIG. 13: The invariant mass distribution of the $B_c^+ \to J/\psi\mu^+$ candidate events using the full CDF data sample with a Monte Carlo simulated signal sample and the calculated backgrounds superimposed. Misid. Muon contains both the misidentified muon and the "double fake" correction. The $B_c^+ \to J/\psi\mu^+\nu$ Monte Carlo simulation shows the shape of the simulated $B_c^+ \to J/\psi\mu^+\nu$ decays, while the number of events is consistent with the B_c^+ excess. The error bars are the statistical uncertainties of the data and background predictions combined.

VI. RELATIVE EFFICIENCY

The ratio of the production cross section times branching ratio of the $B_c^+ \to J/\psi\mu^+\nu$ relative to the $B^+ \to J/\psi K^+$ can be written as

$$\frac{\sigma(B_c^+) * BR(B_c^+ \to J/\psi\mu^+\nu)}{\sigma(B^+) * BR(B^+ \to J/\psi K^+)} = \frac{N_{B_c^+}}{N_{B^+}} \times \epsilon_{rel}, \tag{4}$$

where $N_{B_c^+}$ is finalized in Table VI within the signal mass region ($4-6$ GeV/c^2), the N_{B^+} is given in Fig. 2 (right) and $\epsilon_{rel} = \frac{\epsilon_{B^+}}{\epsilon_{B_c^+} \times \epsilon_{CMUP}}$. Here ϵ_{B^+} is the CDF acceptance for $B^+ \to J/\psi K^+$ decay, $\epsilon_{B_c^+}$ is the CDF acceptance for $B_c^+ \to J/\psi\mu^+\nu$ decay, ϵ_{CMUP} is the third muon detection efficiency by the CMUP detectors. As the CMUP efficiency we use 0.962 ± 0.007(stat)± 0.021 (sys) [10]. This efficiency is normalized to the Monte Carlo simulation.

As an input spectrum for the $B^+ \to J/\psi K^+$ acceptance, the FONLL spectrum from Ref. [11] is used. We find that the FONLL spectrum shows some discrepancies in the low p_T region with respect to the our data. Thus, a corrected FONLL spectrum was used to determine the $B^+ \to J/\psi K^+$ acceptance.

As the input spectrum for the B_c^+, a theoretically-predicted spectra from Ref. [12] is used. Here we also use our background subtracted data to make some corrections in the low p_T region. Comparison of the corrected theoretically-predicted spectra with our data for the $B^+ \to J/\psi K^+$ and for the

$B_c^+ \to J/\psi\mu^+\nu$ decays are shown in Fig. 14

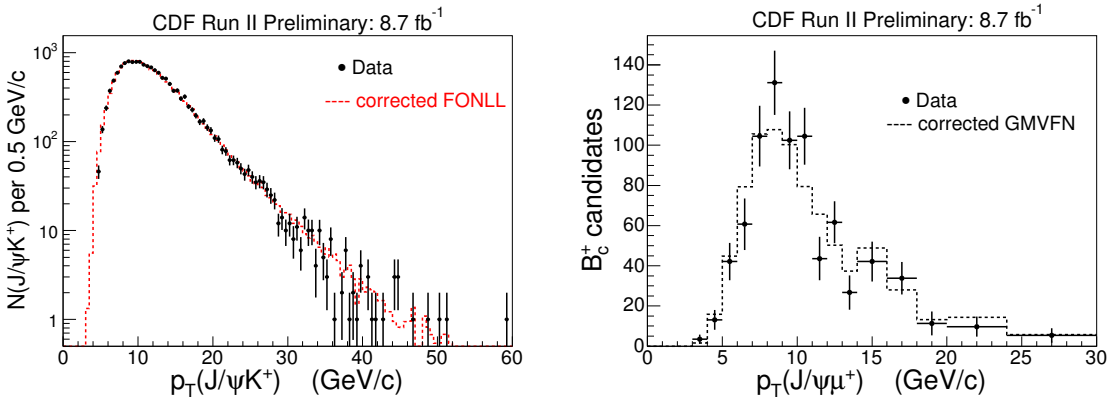

FIG. 14: The left plot illustrates the p_T spectra for $J/\psi K^+$ and the right plot - for the $J/\psi\mu$ samples. Both plots have been background subtracted. Both the theoretically-predicted spectra are corrected using our data.

In the acceptance calculation for both $B_c^+ \to J/\psi\mu^+\nu$ and $B^+ \to J/\psi K^+$ decays we also take into account the fact that XFT efficiencies for kaons and muons, which exist in the data, due to the number of hits required by the XFT in the COT, are not well modeled in the simulation [13].

Finally, the result for $\epsilon_{rel} = \frac{\epsilon_{B^+}}{\epsilon_{B_c^+} \times \epsilon_{CMUP}}$ with $p_T(B) > 6$ GeV/c cut within the $|y|$ <0.6 range is 4.093±0.038 (stat.).

VII. SYSTEMATIC UNCERTAINTIES

We divide the systematic uncertainties into two categories. The first represents the uncertainties on the number of B_c^+ signal events $N_{B_c^+}$. This includes the B_c^+ background systematic uncertainties. The second represents the uncertainties in the relative efficiency. In this case we consider the ϵ_{rel} variations due to uncertainties in the knowledge of the B_c^+ lifetime and production spectrum, the B^+ production spectrum, the relative efficiencies of kaons and muons due to triggering effects at the first level of the CDF II trigger (XFT), and the muon efficiency.

A. B_c^+ background systematics

Below we discuss the following B_c^+ background systematics:

- Misidentified J/ψ
  - As this is derived from data, we do not assign a systematic uncertainty.
- Misidentified muon
  - See discussions in Section III B. Results are given in Table I.
- $b\bar{b}$ background
  - See discussions in Section III C.
- Other decay modes

– The difference between two predictions on BR($B_c^+ \to J/\psi\mu^+\nu$) ([8] and [9]) is 9%. This lead to the systematic uncertainty at the level of 2.2% of $N_{B_c^+}$ or 16.3 events.

Table VII summarizes all B_c^+ background systematics assigned.

B_c^+ background	Systematic uncertainty
Misidentified μ	$^{+9.6}_{-16.5}$
Doubly misidentified	$^{+0.5}_{-0.9}$
$b\bar{b}$	± 5.8
Other decay modes	± 16.3
Total	$^{+19.8}_{-23.9}$

TABLE VII: Systematic uncertainties assigned for various backgrounds.

B. Relative efficiency systematics

We consider following sources of uncertainty:

- B_c^+ lifetime
- B_c^+ production spectrum
- B^+ production spectrum
- K and μ differences in XFT simulation
- CMUP efficiency

The total ϵ_{rel} systematic uncertainty are summarized in Table VIII. Details of the different systematic uncertainties are given in the following sections.

Variation variable	Systematic uncertainty
B_c^+ lifetime	$^{+0.134}_{-0.147}$
B_c^+ spectrum	$^{+0.356}_{-0.303}$
B^+ spectrum	± 0.055
XFT trigger	± 0.070
CMUP efficiency	$^{+0.092}_{-0.087}$
Total	$^{+0.401}_{-0.359}$

TABLE VIII: ϵ_{rel} systematic uncertainties.

1. B_c^+ *lifetime systematics*

The B_c^+ lifetime systematic uncertainty is estimated by varying the B_c^+ lifetime within ± 9 μm relative to the world average value, $c\tau(B_c^+) = 137$ μm. To determine the systematic uncertainty, we generate two B_c^+ Monte Carlo samples with B_c^+ lifetimes, $c\tau(B_c^+)$, of 128 μm and 146 μm.

2. B_c^+ and B^+ production spectrum systematic uncertainties

For both the B_c^+ and B^+ production spectrum systematic uncertainty calculation, we applied a similar approach: the systematic uncertainty is derived from comparing the p_T spectrum given by the data directly with that of simulated events in the detector produced from the corrected theoretical input production spectra. The data to Monte Carlo ratio plots for both cases are used to estimate an average ratio for $p_T(B) > 6$ GeV/c: $\bar{R} = \frac{\sum w_i \times R_i}{\sum w_i}$, where $w_i = \frac{1}{\sigma^2}$ and $\sigma_{\bar{R}} = \sqrt{\frac{\sum \sigma^2}{n(n-1)}}$. Thus, we find $\bar{R}(B_c^+) = 1.00 \pm 0.08$ and $\bar{R}(B^+) = 0.999 \pm 0.0133$. We assign a systematic uncertainties of 8% and 1.3% for the B_c^+ and B^+, respectively. The B_c^+ and B^+ spectrum systematic uncertainties are shown in Table VIII.

3. K and μ differences in XFT simulation

K and μ differences in the XFT simulation are taken into account in the CDF detector acceptance calculation for both $B_c^+ \to J/\psi\mu^+\nu$ and $B^+ \to J/\psi K^+$ decays in Section VI. We find that the ϵ_{rel} difference between using and not using the XFT correction is ± 0.140, and 50% of this difference was assigned as the systematic uncertainty.

C. $\frac{\sigma(B_c^+)*BR(B_c^+\to J/\psi\mu^+\nu)}{\sigma(B^+)*BR(B^+\to J/\psi K^+)}$ ratio systematic uncertainties

The total systematic uncertainty for the $\frac{\sigma(B_c^+)*BR(B_c^+\to J/\psi\mu^+\nu)}{\sigma(B^+)*BR(B^+\to J/\psi K^+)}$ ratio are summarized in Table IX.

Variation variable	Systematic uncertainty
B_c^+ background	$^{+0.0057}_{-0.0068}$
ϵ_{rel}	$^{+0.0207}_{-0.0185}$
Total	$^{+0.0214}_{-0.0197}$

TABLE IX: Systematic uncertainties for $\frac{\sigma(B_c^+)*BR(B_c^+\to J/\psi\mu^+\nu)}{\sigma(B^+)*BR(B^+\to J/\psi K^+)}$ ratio.

VIII. CROSS SECTION RESULTS

Using B_c^+ and B^+ yields from Table VI and Fig. 2 (right), respectively, and the ϵ_{rel} we calculate the ratio of the production cross section time branching ratio of the $B_c^+ \to J/\psi\mu^+\nu$ relative to the $B^+ \to J/\psi K^+$. The final cross section is presented in Table X.

Quantity	Value
$N(B_c^+ \to J/\psi\mu^+\nu)$	739.5 ± 39.6(stat) $^{+19.8}_{-23.9}$(sys)
$N(B^+ \to J/\psi K^+)$	14338 ± 125 (stat)
ϵ_{rel}	4.093 ± 0.038(stat)$^{+0.401}_{-0.359}$(sys)
$\frac{\sigma(B_c^+)*BR(B_c^+\to J/\psi\mu^+\nu)}{\sigma(B^+)*BR(B^+\to J/\psi K^+)}$	0.211 ± 0.012(stat) $^{+0.021}_{-0.020}$ (sys)

TABLE X: Results of B_c^+ production cross section times the branching ratio to $J/\psi\mu^+ + \nu$ over B^+ production cross section times the branching ratio to $J/\psi K^+$.

IX. CONCLUSION

We have performed a measurement of the ratio $\frac{\sigma(B_c^+)*BR(B_c^+\to J/\psi\mu^+\nu)}{\sigma(B^+)*BR(B^+\to J/\psi K^+)}$ using the complete CDF dataset. We have identified a sample of 1370 events with an estimated background from all sources of 630.5 ± 14.2 events. We obtain for $p_T > 6$ GeV/c and $|y| < 0.6$

$$\frac{\sigma(B_c^+) * BR(B_c^+ \to J/\psi\mu^+\nu)}{\sigma(B^+) * BR(B^+ \to J/\psi K^+)} = 0.211 \pm 0.012 \text{ (stat.)}^{+0.021}_{-0.020} \text{ (syst.)}$$

[1] Charge-conjugate states are implied throughout the paper unless otherwise specified.
[2] F. Abe et al. (CDF Collaboration), Phys. Rev. Lett. **81**, 2432 (1998);
F. Abe et al. (CDF Collaboration), Phys. Rev. D **58**, 112004, (1998).
[3] http://www-cdf.fnal.gov/physics/new/bottom/050330.blessed-bc-jpsimu/.
[4] http://www-cdf.fnal.gov/physics/new/bottom/051029.blessed-BcJpsiE/.
[5] http://www-cdf.fnal.gov/physics/new/bottom/090305.blessed-bc-slXsec/.
[6] Mark Patrick Hartz, FERMILAB-THESIS-2008-82 (2008).
[7] R. Aaij et al. (LHCb Collaboration) (2012), hep-ph/1203.3592.
[8] V. V. Kiselev (2003), hep-ph/0308214.
[9] M. A. Ivanov, J. G. Korner, and P. Santorelli, Phys. Rev. D **73**, 054024 (2006).
[10] A. Abulencia et al. (CDF Collaboration), J. Phys. **G34**, 2457 (2007).
[11] M. Cacciari, S. Frixione, M. L. Mangano, P. Nason, and G. Ridolfi, JHEP **07**, 033 (2004).
[12] C.-H. Chang, C.-F. Qiao, J.-X. Wang, and X.-G. Wu, Phys. Rev. D **72**, 114009 (2005).
[13] Karen Ruth Gibson, FERMILAB-THESIS-2006-09 (2006).